DALTON
FULL PAPER

Two new hexanuclear iron(III) complexes with $S = 5$ ground states

Cristina Cañada-Vilalta,[a] Evan Rumberger,[b] Euan K. Brechin,[a] Wolfgang Wernsdorfer,[c] Kirsten Folting,[a] Ernest R. Davidson,[a] David N. Hendrickson*[b] and George Christou*†[a]

[a] *Dept. of Chemistry and the Molecular Structure Center, Indiana University, Bloomington, IN 47405-7102, USA. E-mail: Christou@chem.ufl.edu*
[b] *Department of Chemistry-0358, University of California at San Diego, La Jolla, CA 92093-0358, USA*
[c] *Laboratoire Louis Néel-CNRS, BP166, 25 Avenue des Martyrs, 38042 Grenoble, Cedex 9, France*

Received 20th May 2002, Accepted 13th August 2002
First published as an Advance Article on the web 2nd October 2002

The synthesis and magnetic properties of two new hexanuclear iron complexes $[Fe_6O_2(OH)_2(O_2CR)_{10}L_2]$ (R = Bu^t (**3**), Me (**4**); LH = 2-(2-hydroxyethyl)pyridine (hepH) (**3**), 6-methyl-2-(hydroxymethyl)pyridine (Me-hmpH) (**4**)) are reported. Both compounds are prepared by treatment of $[Fe_3O(O_2CR)_6(H_2O)_3]^+$ with three equivalents of LH in MeCN. The X-ray crystal structure of **3**·2$CHCl_3$·2H_2O is presented. It consists of a planar array of six Fe^{3+} ions comprising two $[Fe_3(\mu_3\text{-}O)]$ subunits that are related by an inversion centre and linked at two of their apices, each linkage consisting of one μ-hydroxo and two μ-carboxylato groups. DC magnetic susceptibility measurements at 1.0 and 0.10 Tesla in the 2.0–300 K range show an increase in the effective magnetic moment with decreasing temperature, corresponding to a high spin (S) ground state. The spin of the ground state was established by magnetization measurements in the 1.0–7.0 T field range and 1.7–4.0 K temperature range. Fitting of the reduced magnetization data by full matrix diagonalization, incorporating both axial and rhombic anisotropy, gave $S = 5$, $g = 1.96$, $D = 0.46$ cm^{-1} and $|E| = 0.046$ cm^{-1} for **3**, and $S = 5$, $g = 2.07$, $D = 0.27$ cm^{-1} and $|E| = 0$ cm^{-1} for **4**. Alternative fits with a negative ZFS were rejected based on their relative fitting error as well as on measurements of the magnetization relaxation behaviour of the complexes at very low temperature (≥0.04 K), where no hysteresis characteristic of a single-molecule magnet was observed.

Introduction

Polynuclear iron(III) complexes have been of interest from a variety of viewpoints and have thus been actively explored for many years. One area to which they are relevant is the protein ferritin, which is involved in the storage and recycling of iron. It contains a highly symmetrical spherical shell consisting of 24 polypeptide subunits and can encapsulate up to *ca.* 4500 Fe atoms in an iron oxide hydroxide core.[1,2] A variety of high nuclearity iron complexes have thus been synthesized and studied as models for the aggregation of the ferritin core.[3–7]

Another interesting aspect of polynuclear iron clusters is their potential to possess large spin (S) values in their ground states, leading to the occasional identification of iron-containing single-molecule magnets (SMMs).[8,9] These are molecules displaying slow magnetization relaxation rates and which, below a certain ('blocking') temperature, can function as single-domain magnetic particles of nanoscale dimensions.[10] To be a SMM, a complex must possess both a significantly large S value and a significant magnetoanisotropy of the easy-axis type, as reflected in a negative zero-field splitting (ZFS) parameter D. These result in a barrier to thermally-activated magnetization reversal of $S^2|D|$ or $(S^2 - \frac{1}{4})|D|$ for integer and half-integer spin, respectively. In fact, these give the upper limit of the barrier size; in practice, it is smaller due to the presence of quantum tunnelling of magnetization (QTM).[8]

For both the above reasons, we have long held an interest in Fe_x cluster chemistry. In the present report, we describe two new Fe_6 complexes prepared from the reaction of $[Fe_3O(O_2CR)_6L_3]^+$ (R = Me, Bu^t; L = py, H_2O) complexes with 2-(2-hydroxyethyl)-pyridine (hepH) and 6-methyl-(2-hydroxymethyl)pyridine (Me-hmpH). These groups have not been used in such reactions before, and they have yielded two new Fe_6 products, both of which have $S = 5$ ground states. We describe their syntheses, structures and magnetic properties.

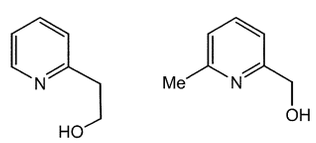

hepH Me-hmpH

Experimental

Syntheses

All manipulations were performed under aerobic conditions using chemicals as received, unless otherwise stated. $[Fe_3O(O_2CBu^t)_6(H_2O)_3](NO_3)$ (**1**)[11] and $[Fe_3O(O_2CMe)_6(py)_3](ClO_4)$ (**2**)[12] were prepared as described in the literature; hepH is 2-(2-hydroxyethyl)pyridine; Me-hmpH is 6-methyl-2-(hydroxymethyl)pyridine.

$[Fe_6O_2(OH)_2(O_2CBu^t)_{10}(hep)_2]$ (3). An orange-red solution of complex **1** (0.500 g, 0.552 mmol) in MeCN (20 mL) was treated with solid hepH (0.204 g, 1.657 mmol) and the solution stirred overnight at room temperature, during which time an orange precipitate was obtained. This was collected by filtration, re-dissolved in $CHCl_3$ (10 mL), filtered, and the filtrate allowed to stand at room temperature. Brown crystals of **3**·2$CHCl_3$·

† Present address: Department of Chemistry, University of Florida, Gainesville, FL 32611-7200, USA.

DOI: 10.1039/b204903a

$2H_2O$ formed over 2 days in 50% yield. The vacuum-dried solid analysed as solvent-free. Anal. calc. (Found) for $C_{64}H_{108}Fe_6N_2O_{26}$: C, 46.40 (46.54); H, 6.57 (6.41); N, 1.69 (1.81)%. Selected IR data (cm^{-1}): 1601(m); 1564(vs); 1483(s); 1458(m); 1421(vs); 1377(m); 1361(m); 1228(s); 1113(w); 1086(m); 787(w); 754(m); 673(m); 605(m); 588(m); 540(m); 503(m); 434(m).

$[Fe_6O_2(OH)_2(O_2CMe)_{10}(Me\text{-}hmp)_2]$ (4). An orange-red solution of complex **2** (560 mg, 0.64 mmol) in MeCN (60 mL) was treated with solid Me-hmpH (239 mg, 1.94 mmol) to give a colour change to dark brown/red. The solution was stirred for 35 min and then evaporated under reduced pressure to dryness. The oily residue was dissolved in CH_2Cl_2 (100 mL), filtered, and the filtrate set aside to slowly evaporate. After four days, red parallelopiped-shaped crystals were obtained. The crystals were collected by filtration, washed with EtOH, and dried *in vacuo*. Yield, 47%. Anal. calc. (Found) for $C_{34}H_{48}Fe_6N_2O_{26}$: C, 33.04 (32.49); H, 3.91 (3.52); N, 2.26 (2.24)%. Selected IR data (KBr, cm^{-1}): 3452(w, b), 2929(w), 1571(vs), 1429(s), 1352(m), 1118(w), 1093(m), 1022(w), 783(w), 653(m), 617(w), 545(m).

X-Ray crystallography and solution of structure

Data were collected using a locally-modified Picker four-circle diffractometer. A suitable crystal of **3**·$2CHCl_3$·$2H_2O$ was attached to a glass fibre using silicone grease and transferred to the goniostat where it was cooled to 112 K for characterization and data collection. A preliminary search of reciprocal space revealed a triclinic unit cell; the choice of the space group $P\bar{1}$ was confirmed by the subsequent solution and refinement of the structure. Following data collection and an analytical absorption correction, data processing gave a unique set of 8153 intensities and $R_{av} = 0.028$ for the averaging of 8145 data measured more than once ($h = \pm16$, $k = \pm17$, and $l = \pm16$).

The structure was solved using a combination of direct methods (MULTAN78)[13] and Fourier techniques. The asymmetric unit contains half of the Fe6 complex, one molecule of chloroform and one molecule of water, O(57). Disorder was observed in one of the *tert*-butyl groups, where atoms C(47), C(48) and C(49) refined to 60% occupancy while C(50), C(51) and C(52) refined to 40% occupancy. All hydrogen atoms (except for those on the disordered atoms and the OH^- groups) were introduced in fixed idealized positions with isotropic thermal parameters equal to 1.0 plus the isotropic equivalent of the parent atom. The final least-squares refinement was carried out using anisotropic thermal parameters on all atoms except C(47)–C(53). The final $R(F)$ was 0.04 for 480 variables and the full unique data; however, data with $F < 3.0\sigma(F)$ were given zero weight. The final difference Fourier map was essentially featureless, the largest peak being 1.1 e $Å^{-3}$ near C(49), and the deepest hole being -0.37 e $Å^{-3}$. Table 1 lists the unit cell and structure refinement data for **3**.

CCDC reference number 186281.

See http://www.rsc.org/suppdata/dt/b2/b204903a/ for crystallographic data in CIF or other electronic format.

Other studies

Infrared spectra were recorded in the solid state (KBr pellets) on a Nicolet Model 510P FTIR spectrophotometer in the 4000–400 cm^{-1} range. Elemental analyses (C, H and N) were performed on a Perkin Elmer 2400 Series II Analyzer. Magnetic measurements were performed on a Quantum Design MPMS-XL SQUID magnetometer equipped with a 7 T magnet at Indiana, or a MPMS5 SQUID magnetometer equipped with a 5.5 T magnet at San Diego. Pascal's constants were used to estimate the diamagnetic correction, which was subtracted from the experimental susceptibility to give the molar magnetic susceptibility (χ_M).

Table 1 Crystallographic data for $[Fe_6O_2(OH)_2(O_2CBu^t)_{10}(hep)_2]$ (**3**)

Formula[a]	$C_{66}H_{112}Cl_6Fe_6N_2O_{28}$
FW	1929.41
Space group	$P\bar{1}$
a/Å	13.968(2)
b/Å	14.434(2)
c/Å	13.567(2)
α/°	113.66(1)
β/°	112.12(1)
γ/°	87.55(1)
V/Å^3	2302.09
Z	1
D_c/g cm^{-3}	1.392
T/°C	−161
Radiation/Å[b]	0.71073
μ/cm^{-1}	11.624
R (R_w)[c](%)	3.98 (4.71)

[a] Including solvate molecules. [b] Graphite monochromator. [c] $R = 100\Sigma||F_o| - |F_c||/\Sigma|F_o|$; $R_w = 100[\Sigma w(|F_o| - |F_c|)^2/\Sigma w|F_o|^2]^{1/2}$, where $w = 1/\sigma^2(|F_o|)$.

Results and discussion

Syntheses

Many synthetic procedures to Fe_x clusters rely on the reaction of $[Fe_3O(O_2CR)_6L_3]^+$ complexes with a potentially chelating ligand,[14] and this was the procedure chosen in the present work. Thus, $[Fe_3O(O_2CBu^t)_6(H_2O)_3](NO_3)$ (**1**) was treated with three equivalents of hepH in MeCN, and this successfully produced a higher nuclearity product, hexanuclear $[Fe_6O_2(OH)_2(O_2CBu^t)_{10}(hep)_2]$ (**3**), in 50% overall yield after recrystallization. Its formation is summarized in eqn. (1).

$$2[Fe_3O(O_2CBu^t)_6(H_2O)_3]^+ + 2\,hepH \longrightarrow [Fe_6O_2(OH)_2(O_2CBu^t)_{10}(hep)_2] + 2\,Bu^tCO_2H + 4\,H_2O + 2\,H^+ \quad (1)$$

The excess of hepH employed over that required by eqn. (1) obviously did not prove detrimental to the formation of an Fe_6 product, and in fact might have been beneficial in providing H^+ acceptors to facilitate formation of OH^- groups. We have not explored reactions using different Fe_3:hepH ratios. Complex **3** was crystallographically characterized.

Similarly, the reaction of $[Fe_3O(O_2CMe)_6(py)_3](ClO_4)$ with three equivalents of Me-hmpH led to formation of $[Fe_6O_2(OH)_2(O_2CMe)_{10}(Me\text{-}hmp)_2]$ (**4**) in 47% overall yield, as summarized in eqn (2).

$$2[Fe_3O(O_2CMe)_6(py)_3]^+ + 2\,Me\text{-}hmpH + 2\,H_2O \longrightarrow [Fe_6O_2(OH)_2(O_2CMe)_{10}(Me\text{-}hmp)_2] + 4\,pyH^+ + 2\,MeCO_2^- + 2\,py \quad (2)$$

Numerous attempts to characterize this product crystallographically were unsuccessful. The corresponding hmp^- complex is not known, but the analytical data that establish the formula of **4**, and the magnetic properties ($S = 5$; see below) that establish its close similarity to **3**, lead us to conclude that it is structurally similar to **3** but with the Me-hmp^- chelate at the positions occupied by the hep^- ligands. Note that the reaction of three equivalents of the less bulky hmpH with $[Fe_3O(O_2CR)_6(H_2O)_3]^+$ (R = Ph, Bu^t) had previously been found to give $[Fe_6O_2(O_2CR)_6(hmp)_6]^{2+}$ complexes with $S = 0$ and a $[Fe_6(\mu_3\text{-}O)_2]$ octahedral core comprising two face-to-face $[Fe_3(\mu_3\text{-}O)]$ triangular units.[14] Thus, they are very different from **3** and **4** in formulation, structure and magnetic properties.

Structural description of $[Fe_6O_2(OH)_2(O_2CBu^t)_{10}(hep)_2]$·$2CHCl_3$·$2H_2O$

A labelled ORTEP[15] plot of complex **3** is presented in Fig. 1, and selected bond distances and angles are listed in Table 2.

Table 2 Selected interatomic distances (Å) and angles (°) for $[Fe_6O_2(OH)_2(O_2CBu^t)_{10}(hep)_2]$ (**3**)

Fe(1)–O(4)	1.900 (2)	Fe(2)–O(22)	2.068(2)
Fe(1)–O(14)	1.972(2)	Fe(2)–O(29)	2.011(2)
Fe(1)–O(15)	2.039(2)	Fe(3)–O(4)	1.884(2)
Fe(1)–O(36)	2.026(2)	Fe(3)–O(5′)	1.979(2)
Fe(1)–O(43)	2.009(2)	Fe(3′)–O(5)	1.979(2)
Fe(1)–N(6)	2.20(3)	Fe(3)–O(24)	2.054(2)
Fe(2)–O(4)	1.961(2)	Fe(3)–O(31)	2.057(3)
Fe(2)–O(5)	1.947(2)	Fe(3)–O(38)	2.054(3)
Fe(2)–O(14)	2.001(2)	Fe(3)–O(45)	2.029(2)
Fe(2)–O(17)	2.063(2)	Fe(1)–Fe(2)	2.933(2)
O(5)–O(22′)	2.821(2)	Fe(1)–Fe(3)	3.253(2)
		Fe(2)–Fe(3)	3.570(2)
O(4)–Fe(1)–O(14)	81.5(1)	O(5)–Fe(2)–O(29)	90.8(1)
O(4)–Fe(1)–O(15)	94.6(1)	O(14)–Fe(2)–O(17)	88.8(1)
O(4)–Fe(1)–O(36)	96.2(1)	O(14)–Fe(2)–O(22)	88.6(1)
O(4)–Fe(1)–O(43)	100.2(1)	O(14)–Fe(2)–O(29)	93.7(1)
O(4)–Fe(1)–N(6)	168.9(1)	O(17)–Fe(2)–O(22)	174.8(1)
O(14)–Fe(1)–O(15)	89.1(1)	O(17)–Fe(2)–O(29)	87.0(1)
O(14)–Fe(1)–O(36)	96.5(1)	O(22)–Fe(2)–O(29)	88.7(1)
O(14)–Fe(1)–O(43)	174.6(1)	O(4)–Fe(3)–O(5′)	93.5(1)
O(14)–Fe(1)–N(6)	87.6(1)	O(4)–Fe(3)–O(24)	92.9(1)
O(15)–Fe(1)–O(36)	168.4(1)	O(4)–Fe(3)–O(31)	176.5(1)
O(15)–Fe(1)–O(43)	85.7(1)	O(4)–Fe(3)–O(38)	94.9(1)
O(15)–Fe(1)–N(6)	82.8(1)	O(4)–Fe(3)–O(45)	96.9(1)
O(36)–Fe(1)–O(43)	88.4(1)	O(5′)–Fe(3)–O(24)	98.50(9)
O(36)–Fe(1)–N(6)	87.3(1)	O(5′)–Fe(3)–O(31)	85.1(1)
O(43)–Fe(1)–N(6)	90.5(1)	O(5′)–Fe(3)–O(38)	88.22(9)
O(4)–Fe(2)–O(5)	96.2(1)	O(5′)–Fe(3)–O(45)	168.8(1)
O(4)–Fe(2)–O(14)	79.3(1)	O(24)–Fe(3)–O(31)	84.1(1)
O(4)–Fe(2)–O(17)	92.3(1)	O(24)–Fe(3)–O(38)	169.4(1)
O(4)–Fe(2)–O(22)	91.69(9)	O(24)–Fe(3)–O(45)	85.2(1)
O(4)–Fe(2)–O(29)	173.0(1)	O(31)–Fe(3)–O(38)	88.3(1)
O(5)–Fe(2)–O(14)	175.4(1)	O(31)–Fe(3)–O(45)	84.7(1)
O(5)–Fe(2)–O(17)	90.51(9)	O(38)–Fe(3)–O(45)	86.7(1)
O(5)–Fe(2)–O(22)	92.46(9)	Fe(2)–O(4)–Fe(3)	136.4(1)
Fe(1)–O(4)–Fe(2)	98.9(1)	Fe(2)–O(5)–Fe(3)′	121.6(1)
Fe(1)–O(4)–Fe(3)	118.6(1)	Fe(1)–O(14)–Fe(2)	95.2(1)

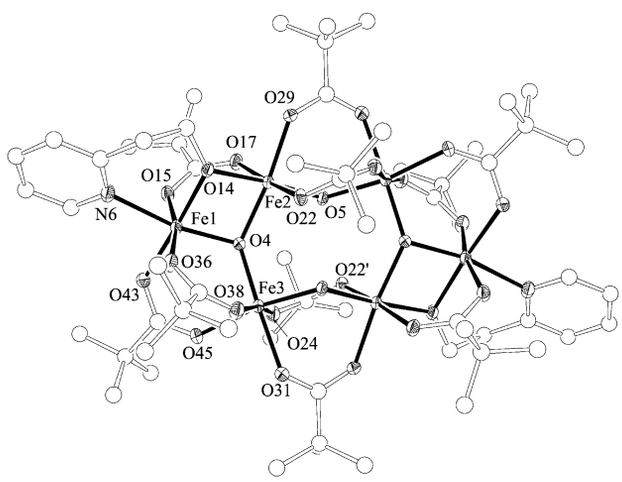

Fig. 1 ORTEP representation of $[Fe_6O_2(OH)_2(O_2CBu^t)_{10}(hep)_2]$ (**3**) with the atoms drawn at the 50% probability level. Hydrogen atoms have been omitted for clarity.

Complex **3** crystallizes in the triclinic space group $P\bar{1}$ and has crystallographic C_i symmetry, the asymmetric unit containing only three iron atoms.

The structure consists of an almost planar array of six Fe atoms (the mean deviation from the least-squares plane being 0.0122 Å). The core can be described as comprising two trinuclear $[Fe_3(\mu_3\text{-}O)]^{7+}$ units linked at two of their apices. Each linkage is by one μ-OH^- and two μ-$Bu^tCO_2^-$ bridges. The angle at the bridging hydroxide oxygen atom, O(5), is 121.6(1)°. The three Fe atoms of each triangular unit are bridged by two μ-$Bu^tCO_2^-$ groups between Fe(1) and Fe(3), and by one μ-$Bu^tCO_2^-$ group and a μ-alkoxo group from an hep^- ligand between Fe(1) and Fe(2). Octahedral coordination at Fe(1) is completed by the nitrogen atom of the same hep^- group, which is therefore forming a six-membered chelate ring at Fe(1) and at the same time bridging Fe(1) and Fe(2).

The three Fe–O(4) bond distances and Fe–O(4)–Fe angles within each trinuclear unit are inequivalent, and the triangles are thus scalene. This is also reflected in the different Fe ··· Fe distances: the shortest is Fe(1) ··· Fe(2) (2.933 Å), which is bridged by the alkoxo and a carboxylate group; the longest is Fe(2) ··· Fe(3) (3.570 Å), which has no bridges other than O(4); and the intermediate distance is Fe(1) ··· Fe(3) (3.253 Å), which has two carboxylate bridges . The oxide atom O(4) is 0.267 Å below the Fe(1)/Fe(2)/Fe(3) least-squares plane.

The 2.821(2) Å separation between the μ-hydroxo atom O(5) and an oxygen atom O(22′) of the distal μ-$Bu^tCO_2^-$ group indicates the presence of an intramolecular hydrogen bond. Minimization of this separation appears to be the cause of the clearly observable twist of this carboxylate group. The structure of **3** is overall fairly similar to those of previously reported $[Fe_6O_2(OH)_2(O_2CMe)_{10}(C_{10}H_{13}N_4O)_2]$[14] and $[Fe_6O_2(OH)_2(O_2CMe)_{10}(C_7H_{11}N_2O)_2]$.[16]

Magnetochemistry

Variable temperature dc magnetic susceptibility studies were performed on powdered samples of compounds **3** and **4**, restrained in eicosane to prevent torquing, in applied dc magnetic fields of 1.0 and 0.10 T (10 and 1.0 kG), respectively, in the 2.0–300 K range. Plots of the effective magnetic moment versus temperature for **3** and **4** are shown in Figs. 2 and 3, respectively.

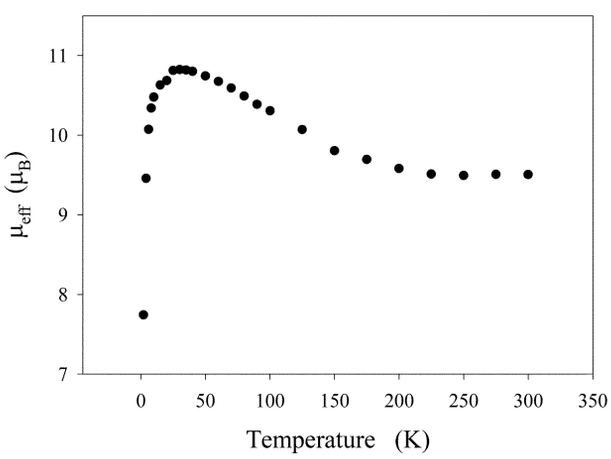

Fig. 2 Plot of the effective magnetic moment (μ_{eff}/Fe_6) *vs.* temperature for complex **3**.

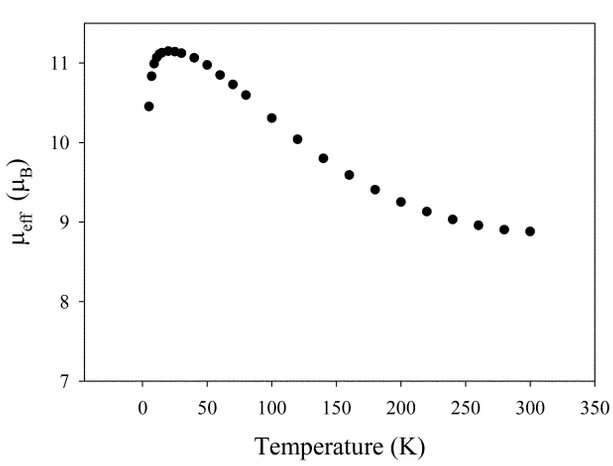

Fig. 3 Plot of the effective magnetic moment (μ_{eff}/Fe_6) *vs.* temperature for complex **4**.

For complex **3**, the effective magnetic moment (μ_{eff}) per Fe_6 cluster steadily increases from 9.50 μ_B ($\chi_M T$ = 11.28 cm^3 K mol^{-1}) at 300 K to a maximum of 10.82 μ_B ($\chi_M T$ = 14.63 cm^3 K mol^{-1}) at 30 K and then drops sharply to a value of 7.74 μ_B at 2.0 K. The 300 K value is significantly lower than the 14.49 μ_B ($\chi_M T$ = 26.28 cm^3 K mol^{-1}) expected for six non-interacting Fe^{3+} (S = 5/2) ions with g = 2, indicating the presence of antiferromagnetic interactions. As the temperature decreases, the observed increase in μ_B is consistent with increasing population of a high spin ground state; the maximum value at 30 K is very close to that expected for an S = 5 ground state [10.95 μ_B ($\chi_M T$ = 15 cm^3 K mol^{-1}) for g = 2]. Similar results were obtained for complex **4**. In this case, the μ_{eff} value at 300 K is 8.88 μ_B ($\chi_M T$ = 9.85 cm^3 K mol^{-1}), increasing with decreasing temperature to reach a plateau of 11.14 μ_B ($\chi_M T$ = 15.51 cm^3 K mol^{-1}) at 20–25 K. For both compounds, the rapid decrease in μ_{eff} at very low temperatures is very likely due to zero-field splitting of the S = 5 spin ground state, and perhaps some weak intermolecular interactions.

The spin Hamiltonian describing the exchange interactions in these complexes is given by eqn (3), where S_i refers to the spin of atom Fe_i in Fig. 1.

$$\mathcal{H} = -2J_{12}(\hat{S}_1\hat{S}_2 + \hat{S}_{1'}\hat{S}_{2'}) - 2J_{13}(\hat{S}_1\hat{S}_3 + \hat{S}_{1'}\hat{S}_{3'}) - 2J_{23}(\hat{S}_2\hat{S}_3 + \hat{S}_{2'}\hat{S}_{3'}) - 2J_{23'}(\hat{S}_2\hat{S}_{3'} + \hat{S}_{2'}\hat{S}_3) \quad (3)$$

Unfortunately, a theoretical treatment of the susceptibility data *via* the Kambé method[17] to determine the individual pairwise Fe_2 exchange interactions was not possible owing to the topological complexity and low symmetry of the Fe_6 core. Similarly, a matrix diagonalization approach would involve diagonalizing a 46 656 × 46 656 matrix and was not attempted.

Efforts were instead concentrated only on determining the spin of the ground states of the complexes and the magnitudes of their zero-field splitting (ZFS) by collecting variable-temperature and -field magnetization data. Shown in Figs. 4 and 5 are the magnetization (M) data plotted as reduced magnetization ($M/N\mu_B$) *versus* H/T for complexes **3** and **4**, respectively, where N is Avogadro's number, μ_B is the Bohr magneton, and H is the applied magnetic field. The measurements were carried out on powdered samples (restrained in eicosane) in 1.0 to 7.0 T fields and in the 1.8 to 4.0 K range. At the highest field and lowest temperature, the reduced magnetization for compounds **3** and **4** saturates at values of *ca.* 9.5 and 10.2 μ_B, respectively. These values are very close to the expected saturation value of 10 μ_B for an S = 5 ground state with g = 2, confirming the earlier conclusions from the magnetic susceptibility data. ZFS of the ground state is evident from the fact that the isofield lines do not superimpose. The data sets were each fit to a model that assumes only the ground state is populated in these field and temperature ranges. The data were least-squares fit by diagonalization of the spin Hamiltonian matrix, which includes the Zeeman interaction and axial zero-field splitting, eqn. (4), and calculates the full powder average of the magnetization. For complex **3**, the fit gave S = 5, g = 1.96 and D = 0.50 cm^{-1}.

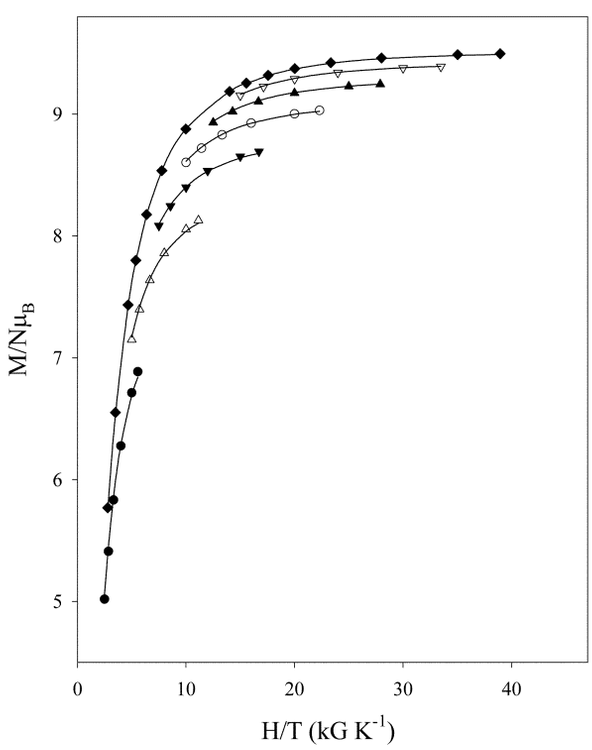

Fig. 4 Plot of the reduced magnetization ($M/N\mu_B$) *vs.* H/T for complex **3** in applied fields of 1 (●), 2 (△), 3 (▼), 4 (○), 5 (▲), 6 (▽) and 7 (◆) Tesla. The solid lines are the fit of the data; see the text for the fitting parameters.

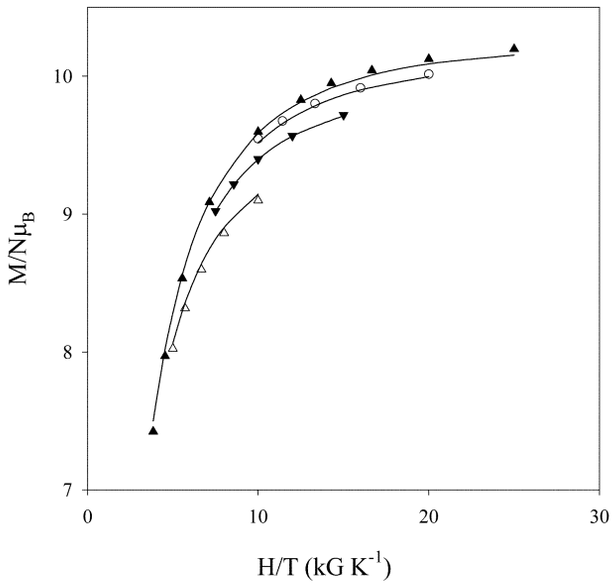

Fig. 5 Plot of the reduced magnetization ($M/N\mu_B$) *vs.* H/T for complex **4** in applied fields of 2 (△), 3 (▼), 4 (○) and 5 (▲) Tesla. The solid lines are the fit of the data; see the text for the fitting parameters.

$$\mathcal{H} = g\mu_B\hat{S}H + D[\hat{S}_Z^2 - 1/3S(S+1)] \quad (4)$$

Comparable fits were obtained with S = 4 and S = 6, but these were rejected because they gave unreasonable g values. It should also be noted that fitting of magnetization data for a given S value usually gives two minima, one with $D > 0$ and one with $D < 0$. The quality of the fit with $D > 0$ was considerably better in this case.

In order to assess whether the values found for $\pm D$ and g truly correspond to the global minima of the fits rather than local minima, the error surfaces for the two fits were calculated. The two-dimensional contour plots in Figs. 6 and 7 clearly show in each case only the two above-mentioned minima with positive and negative D values, and no other fitting minima. Further, since **3** crystallizes in a triclinic space group, and therefore its symmetry is clearly rhombic not axial, the data were also fit using a spin Hamiltonian that also includes a term for the transverse (or rhombic) anisotropy, eqn. (5).

$$\mathcal{H} = g\mu_B\hat{S}H + D[\hat{S}_Z^2 - 1/3S(S+1)] + E(\hat{S}_x^2 - \hat{S}_y^2) \quad (5)$$

The fit improves slightly with the inclusion of the rhombic ZFS parameter E, the fit parameters being S = 5, g = 1.96, D = 0.46 cm^{-1} and $|E|$ = 0.046 cm^{-1}. This fit is shown as the solid lines in Fig.4. Similar results were obtained for complex **4**. In this case,

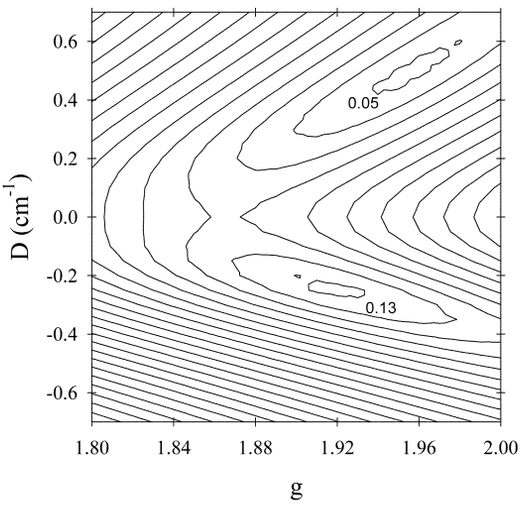

Fig. 6 Two-dimensional contour projection of the fitting error *vs.* g and D surface for the fit of the reduced magnetization data of complex **3**.

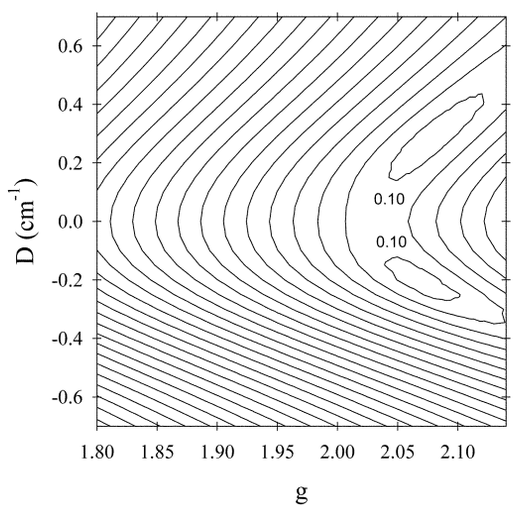

Fig. 7 Two-dimensional contour projection of the fitting error *vs.* g and D surface for the fit of the reduced magnetization data of complex **4**.

the quality of the fit is virtually the same for $D < 0$ and $D > 0$. Only the results for the latter fit are shown, as solid lines in Fig.5. They correspond to $S = 5$, $g = 2.07$, $D = 0.27$ cm^{-1} and $|E| = 0$ cm^{-1}.

The relatively large ground state spin values of **3** and **4** can be assigned to the presence of spin frustration[18] effects, whereby competing antiferromagnetic exchange interactions between the various Fe_2 pairs lead to the spins being prevented (frustrated) from aligning completely antiparallel and yielding an $S = 0$ ground state. Instead, a balance is achieved that depends on the relative magnitude of the competing interactions, giving an $S = 5$ ground state for the present complexes. Such spin frustration effects within the Fe_6 core similar to that found in **3** and **4** have been previously discussed in detail.[16,19]

Since complexes **3** and **4** possess unusually high ground state spin values and significant anisotropy as reflected in their D values, it was of interest to explore the possibility of them displaying behaviour characteristic of a single-molecule magnet (SMM). However, neither complex exhibited an out-of-phase (χ_M'') component of the ac susceptibility down to 1.8 K and with ac oscillation frequencies up to 1500 Hz. A frequency-dependent χ_M'' signal is a diagnostic signal of slow magnetization relaxation rates characteristic of a SMM. Thus, neither complex displays slow (ms) magnetization relaxation at these temperatures. For complex **3**, the behaviour at even lower temperatures was also studied.

Magnetization studies below 1.8 K

If a complex is a SMM below some temperature, then it will exhibit a hysteresis loop in a magnetization *vs.* dc field plot. Such magnetization *vs.* field studies were performed on complex **3** with a micro-SQUID apparatus[20] in the 0.04–3.0 K temperature range, using different sweep rates from 0.018 to 0.070 T s^{-1}. The resulting plots are shown in Figs. 8 and 9. In Fig. 8 are

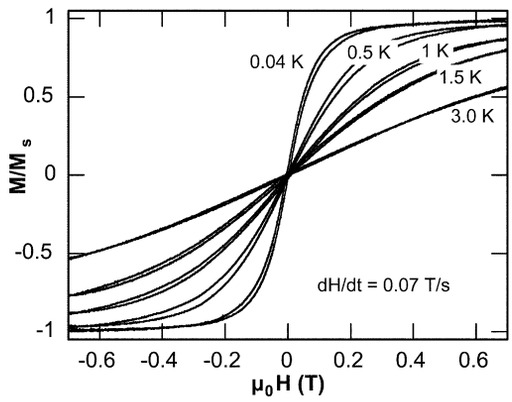

Fig. 8 Magnetization *vs.* field plots of complex **3** at five temperatures and a fixed field sweeping rate of 0.07 T s^{-1}. The magnetization is normalized to its maximum value, M_s.

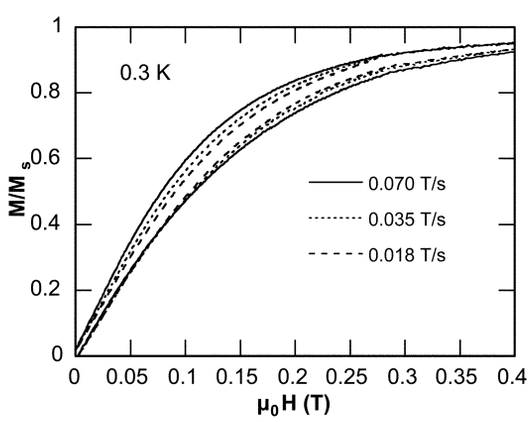

Fig. 9 Magnetization *vs.* field plots of complex **3** at three sweeping rates at 0.3 K. The magnetization is normalized to its maximum value, M_s.

shown the magnetization *vs.* field scans at five temperatures and a constant field sweep rate of 0.07 T s^{-1}. The overall profile does not look like that expected for a magnetic particle such as a SMM with a significant anisotropy barrier to magnetization relaxation. The butterfly-like pattern of the scans and the very slight hysteresis are characteristic not of single-molecule magnetism behaviour but of a phonon-bottleneck; that is, phonon exchange (thermal coupling) between the crystal and its environment (cryostat) is limited, an equilibrium in the phonon density of states cannot be maintained during spin relaxation, and thus the latter is hampered and a small hysteresis is observed. This behaviour was first described in a molecular system for a V_{15} cluster with $S = 1/2$.[21,22] Note that in Fig. 8 there is no change in the separation (coercive field) in the magnetization scans at zero field, consistent with the absence of true hysteresis due to SMM behaviour. This is further emphasized in Fig. 9 where magnetization *vs.* field scans are shown at 0.3 K for different field sweep rates. No change in the coercivity at zero field with scan rate is observed, unlike the behaviour expected for a SMM where the coercivity should increase with increasing scan rates.

The combined results above suggest that complex **3** has no significant barrier to magnetization relaxation and is thus not a SMM. This is consistent with the earlier conclusion that the D

value is positive for this complex. The SMM phenomenon requires a negative D value, *i.e.* easy-axis-type magnetoanisotropy, whereby the two antiparallel orientations of the magnetization vector along the easy axis (say, 'spin up' and 'spin down') are the lower energy ones and there is thus a barrier to interconversion between them *via* intermediate orientations. It should be noted that if the alternative situation (*i.e.* negative D value) was the correct one for **3**, then its $D = -0.26$ cm^{-1} = -0.37 K value would lead to a barrier to magnetization relaxation of $S^2|D| = 6.5$ cm^{-1} = 9.4 K (actually a bit less due to the expected quantum tunnelling effects), a value comparable to that in the Mn_4 SMMs with the $[Mn_4O_3X]^{+6}$ core and an $S = 9/2$ ground state.[23,24] The latter complexes show clear evidence for slow magnetization relaxation, such as out-of-phase (χ_M'') signals above 1.7 K in the ac susceptibility, and hysteresis loops below 1 K with large coercivities.

Conclusions

The use of the chelating ligands 2-(2-hydroxyethyl)pyridine (hepH) and 6-methyl-(2-hydroxymethyl)pyridine (Me-hmpH) in reactions with $[Fe_3O(O_2CR)_6L_3]^+$ has allowed access to two new hexanuclear iron(III) complexes, **3** and **4**. The crystal structure of **3** has been obtained, and it consists of a planar array of six Fe^{3+} ions arranged in two triangular subunits bridged together at two vertices. Analytical and magnetic data indicate that compound **4** is isostructural with **3**. The magnetic properties of these compounds have been investigated, and both have been found to possess $S = 5$ ground states and positive zero-field splitting parameters, D.

The structures of these compounds with hep$^-$ and Me-hmp$^-$ are distinctly different from those previously reported with hmp$^-$, emphasizing the dependence of the product identity on relatively small changes in the chelating ligand employed.

Acknowledgements

This work was supported by the USA National Science Foundation.

References

1 E. C. Theil, in *Handbook of Metalloproteins*, eds. A. Messerschmidt, R. Huber, T. Poulos and K. Wieghardt, Wiley, Chichester, 2001, pp. 771–781.
2 B. Xu and N. D. Chasteen, *J. Biol. Chem.*, 1991, **266**, 19965.
3 B. P. Murch, P. D. Boyle and L. Que, Jr., *J. Am. Chem. Soc.*, 1985, **107**, 6728.
4 A. N. Mansour, C. Thompson, E. C. Theil, N. D. Chasteen and D. E. Sayers, *J. Biol. Chem.*, 1985, **260**, 7975.
5 Q. T. Islam, D. E. Sayers, S. M. Gorun and E. C. Theil, *J. Inorg. Biochem.*, 1989, **36**, 51.
6 K. L. Taft, G. C. Papaefthymiou and S. J. Lippard, *Inorg. Chem.*, 1994, **33**, 1510.
7 R. J. Lachicotte and K. S. Hagen, *Inorg. Chim. Acta*, 1997, **263**, 407.
8 G. Christou, D. Gatteschi, D. N. Hendrickson and R. Sessoli, *MRS Bull.*, 2000, **25**, 66 and refs. cited therein; D. N. Hendrickson, G. Christou, H. Ishimoto, J. Yoo, E. K. Brechin, A. Yamaguchi, E. M. Rumberger, S. M. Aubin, Z. Sun and G. Aromí, *Polyhedron*, 2001, **20**, 1479.
9 D. Gatteschi, R. Sessoli and A. Cornia, *Chem. Commun.*, 2000, **9**, 725 and refs. cited therein.
10 M. Soler, E. Rumberger, K. Folting, D. N. Hendrickson and G. Christou, *Polyhedron*, 2001, **20**, 1365; M. Soler, S. K. Chandra, D. Ruiz, J. C. Huffman, D. N. Hendrickson and G. Christou, *Polyhedron*, 2001, **20**, 1279; S. M. J. Aubin, Z. Sun, H. J. Eppley, E. M. Rumberger, I. A. Guzei, K. Folting, P. Gantzel, A. L. Rheingold, G. Christou and D. N. Hendrickson, *Polyhedron*, 2001, **20**, 1139; E. C. Sañudo, V. A. Grillo, J. Yoo, J. C. Huffman, J. C. Bollinger, D. N. Hendrickson and G. Christou, *Polyhedron*, 2001, **20**, 1269.
11 A. Earnshaw, B. N. Figgis and J. Lewis, *J. Chem. Soc. A*, 1966, 1656.
12 A. M. Bond, R. J. H. Clark, D. G. Humphrey, P. Panayiotopoulos, B. W. Skelton and A. H. White, *J. Chem. Soc., Dalton Trans.*, 1998, **11**, 1845.
13 P. Main, S. E. Hull, L. Lessinger, G. Germain, J. P. Declercq and M. M. Woolfson, MULTAN-78: A System of Computer Programs for the Automatic Solution of Crystal Structures from X-Ray Diffraction Data, University of York, UK, and Louvain, Belgium, 1978.
14 E. K. Brechin, M. J. Knapp, J. C. Huffman, D. N. Hendrickson and G. Christou, *Inorg. Chim. Acta*, 2000, **297**, 389.
15 C. K. Johnson and M. N. Burnett, ORTEP-III, Report ORNL-6895, Oak Ridge National Laboratory, Tennessee, USA, 1996; L. J. Farrugia, *J. Appl. Crystallogr.*, 1997, **30**, 565.
16 C. A. Christmas, H.-L. Tsai, L. Pardi, J. M. Kesselman, P. K. Gantzel, R. K. Chadha, D. Gatteschi, D. F. Jarvey and D. N. Hendrickson, *J. Am. Chem. Soc.*, 1993, **115**, 12483.
17 J. K. Kambé, *J. Phys. Soc. Jpn.*, 1950, **5**, 48.
18 J. K. McCusker, E. A. Schmitt and D. N. Hendrickson, in *Magnetic Molecular Materials*, eds. D. Gatteschi, O. Kahn, J. S. Miller and F. Palacio, Kluwer Academic Publishers, Dordrecht, The Netherlands, 1991, pp. 297–319; E. Libby, J. K. McCusker, E. A. Schmitt, K. Folting, J. C. Huffman, D. N. Hendrickson and G. Christou, *Inorg. Chem.*, 1991, **30**, 3486; J. K. McCusker, H. G. Jang, S. Wang, G. Christou and D. N. Hendrickson, *Inorg. Chem.*, 1992, **31**, 1874.
19 J. K. McCusker, C. A. Christmas, P. M. Hagen, R. K. Chadha, D. F. Jarvey and D. N. Hendrickson, *J. Am. Chem. Soc.*, 1991, **113**, 6114.
20 W. Wernsdorfer, E. Bonet Orozco, K. Hasselbach, A. Benoit, D. Mailly, O. Kubo, H. Nakano and B. Barbara, *Phys. Rev. Lett.*, 1997, **79**, 4014.
21 I. Chiorescu, W. Wernsdorfer, A. Müller, H. Bögge and B. Barbara, *Phys. Rev. Lett.*, 2000, **84**, 3454.
22 I. Chiorescu, W. Wernsdorfer, A. Müller, H. Bögge and B. Barbara, *J. Magn. Magn. Mater.*, 2000, **221**, 103.
23 G. Aromí, S. Bhaduri, P. Artús, K. Folting and G. Christou, *Inorg. Chem.*, 2002, **41**, 805; N. Aliaga, K. Folting, D. N. Hendrickson and G. Christou, *Polyhedron*, 2001, **20**, 1273.
24 S. Wang, M. S. Wemple, J. Yoo, K. Folting, J. C. Huffman, K. S. Hagen, D. N. Hendrickson and G. Christou, *Inorg. Chem.*, 2000, **39**, 1501.